Electron Spin Resonance Studies of Anisotropic Ordering, Spin Relaxation, and Slow Tumbling in Liquid Crystalline Solvents. 4. Cholestane Motions and Surface Anchoring in Smectics

Eva Meirovitch† and Jack H. Freed*

Department of Chemistry, Baker Laboratory, Cornell University, Ithaca, New York 14853 *(Received: February 28, 1980)*

ESR line shape studies of cholestane (CSL) in monodomain liquid crystals of HOAB, 40,6, and 40,8 oriented between glass surfaces are reported. The line shapes are analyzed in terms of the Polnaszek–Bruno–Freed theory for spectra from slow tumbling probes in ordered fluids. Preparation of monodomain smectic crystals, free from previously observed effects of static director distribution due to magnetic torques, and therefore adequate for accurate studies of dynamic line shapes, both as a function of temperature and orientation, is described. CSL exhibits fast motion in HOAB but slow motion in 40,8 and 40,6. In the nematic phases the anisotropy in the diffusion tensor ($N \approx 5$) is consistent with the geometry of the probe molecule, as expected for simple Brownian type of diffusion in a mean potential field. In the smectic phases, an "apparent" anisotropy was found by simulations to be substantially greater than predicted by the molecular configuration and *appears* to be increasing dramatically as the temperature is decreased. It is argued that this is untenable in the context of the model. Instead, it is shown that an approximate model of fluctuating torques could be successfully used to interpret the apparent anomalies. These observations are interpreted in terms of the effect of the local solvent structure on the nature of the overall dynamic mode of the probe, implying considerable local cooperativity in these smectic phases. It is also shown by preliminary studies with the PD-Tempone probe that the very well-aligned samples may experience substantial elastic distortions with magnetic fields of 3 kG when the field is tilted relative to the normal to the plates. Since this is contrary to predictions of previous theory, a new theoretical analysis is given which suggests that (1) the conditions of weak vs. strong anchoring are different in the nematic vs. smectic phases and (2) it is quite possible to have weak anchoring in the smectic phase of a sample which exhibits rather strong anchoring in the nematic phase.

I. Introduction

The rigid CSL probe has been used extensively to study both thermotropic[1-6] and lyotropic[7] smectic liquid crystals. It was found in a recent study[8] of ESR line shapes of this probe in the nematic phase V that this probe often exhibits slow tumbling in nematic and smectic phases. Correlation times greater than 10^{-9} s with $N \approx 5$ [where N is defined as the ratio of $R_{\parallel}$, the component of the rotational diffusion tensor parallel to the long axis of the rigid cylindrical CSL molecule, to $R_{\perp}$, the perpendicular component] were shown to be in the slow tumbling range.[8]

The study of smectic phases, which possess some degree of positional as well as orientational order,[9] is a straightforward extension of previous studies on nematics. Usually the dynamic behavior of a probe molecule in an oriented uniaxial medium can be estimated by adding the effect of an orienting potential to the dynamics for the isotropic phase.[6,8,10,11] Thus, for example, the rotational anisotropy (i.e., N) is about the same in isotropic and nematic phases.[6,11] While this approach is found to be reasonable in studying the motion of weakly ordered probes dissolved in fluid nematic solvents, effects of a slowly relaxing local structure (SRLS) mechanism, indicating coupling between individual probe modes and localized modes of the surrounding solvent, were found to be present.[11] Our results on the spin relaxation of PD-Tempone in the smectic A and B_A phases of *N*-(*p*-butoxybenzylidene)-*p*-*n*-hexylaniline (40,6) and *N*-(*p*-butoxybenzylidene)-*p*-*n*-octylaniline (40,8)[6] were interpreted in terms of significant contributions from this SRLS mechanism. This observation suggests that, with increasing order of the phase investigated, the particular characteristics of the surrounding matrix become manifested to a greater degree in the dynamic behavior of the solute, and this appears to be the case for other studies.[5,12]

Such observations certainly point out the need for examining more carefully the particular characteristics of a highly ordered probe (such as CSL) in a smectic phase with substantial intra- and interlayer molecular organization. This is our main concern in the present report. We also examine to what extent the slow-tumbling theories for probe dynamics in oriented media are applicable to low-temperature smectic phases.

Besides these considerations, there is an aspect peculiar to smectic structures. The behavior of smectic liquid crystals in the presence of an external magnetic field differs from that of nematic liquid crystals in that, once aligned, the smectic director is usually "locked-in"[1-6,11,13] so orientation-dependent ESR measurements can be performed in smectic crystals. However, recent experiments in smectic C monodomains[13,14a] showed that in some cases magnetic instabilities, resulting in reorientation of the director about the normal to the smectic layers, may occur upon tilting the field away from parallel alignment with the smectic C director.[14] However, by decreasing the monodomain thickness to a sufficiently low value (by monitoring the interplate distance), these effects could be suppressed completely.[13,14a]

The study[6] of PD-Tempone in the smectic A and B_A phases of 40,6 and 40,8 revealed that, in the conventional cylindrical-tube sample holders, magnetic torques operating on the smectic director contribute to static inhomogeneous angular-dependent line broadening probably due to splay-type deformations of the smectic layers.[6,15,16] These effects were found to depend upon the size and shape of the sample holder as well as the orientation in the magnetic field. They are expected to be suppressed by preparing strongly anchored monodomains between

† Chaim Weizmann Postdoctoral Fellow.

0022-3654/80/2084-2459$01.00/0

thin-spaced glass surfaces.[13,14] There was an obvious need to have a refined technique for obtaining smectic monodomains free from effects of inhomogeneous line broadening in order to perform orientation-dependent width measurements in smectic liquid crystals. This prompted us to consider the morphology of smectic structures and to refine previous techniques[4,13,14a] for obtaining smectic monodomains adequate for careful ESR line shape studies. Our results included preliminary study on PD-Tempone, which unfortunately plates out rather quickly, and a detailed line shape study on CSL in the various liquid crystalline phases, since the CSL did not plate out in the thin-plate samples. CSL was found to exhibit fast motion in HOAB and the ESR line widths were analyzed by a procedure analogous to that of Lin and Freed.[6] The smectic C phase was studied as a function of orientation at both X and R band. The ESR spectra of CSL in the liquid crystalline phases of 40,6 and 40,8 required a complete line shape analysis due to slow motion.[8,10,11]

Our results on probe dynamics are then compared with models for the motion of liquid crystalline molecules in smectic phases.

We also present in Appendix A a detailed analysis of magnetic-field-induced instabilities in the smectic A phase appropriate for the discussion of our results on smectic A morphology.

II. Experimental Section

A. Preparation of Samples. The liquid crystals 40,8 and HOAB were purchased from Shawnee Chemical Co. and Synvar Associates, respectively, while 40,6 was synthesized by condensing equimolar quantities of 4-*n*-butoxybenzaldehyde and 4-*n*-hexylaniline in absolute ethanol.[17] All liquid crystals were purified by several recrystallizations from absolute ethanol until a constant melting point was achieved. Radical solutions (10^{-3}–10^{-4} M) were prepared by proper weighing. The transition temperatures of the doped liquid crystals were about 2–3 °C (4–5 °C) lower than the literature values for approximately 10^{-4} (10^{-3}) M solutions of both PD-Tempone and CSL.

The nitroxide free radical, perdeuterated 2,2,6,6-tetramethyl-4-piperidinyl 1-oxy (PD-Tempone), was synthesized by standard methods[18] as previously discussed by Hwang et al.[19]

The spin probe spiro[3′,3′-dimethyloxazolidinyl-*N*-oxy-2′,3-5α-cholestane] (CSL) was obtained from Synvar Associates.

We first describe briefly the preparation of CSL-doped smectic C monodomain of HOAB.[4,13,14a] The mesogen was held between glass pieces made of microscope cover slides of width ranging between 2 and 3 mm and length ranging between 5 and 10 mm. (Since both X- and R-band experiments were performed on the same smectic C monodomain, the dimensions of the sample were determined by considerations of dielectric losses at R band.) The glass pieces were previously treated by washing in a mixture of concentrated nitric and sulfuric acids followed by thorough rinsing with distilled water and finally by soaking in ethyl alcohol which was removed by flaming the plates. The clean glass slides were finally soaked in a saturated solution of trimethylhexadecylammonium bromide (from Aldrich) known to induce homeotropic alignment of the liquid crystalline molecules.[20]

A "sandwich" made up of two properly treated glass pieces was subsequently placed on a hot plate warmed to the temperature corresponding to the nematic or isotropic mesophase of HOAB. A drop of liquid crystal was now allowed to flow in between the glass slides. These were then held together by a thin strip of teflon. The thickness of the mesogen in these samples was estimated by a microscope focussing technique to be approximately 20 μm. For X-band experiments the sandwich assembly was attached to a quartz rod which was connected to a goniometer head. For experiments at R band (35 GHz) the sandwiches were glued to the bottom of an ESR cavity with an all-through hole. To align the slides in a vertical position, we used an orienting device designed to enable vertical mounting of the glass surfaces to within 2°.

Oriented samples of smectic C were obtained by cooling the mesogen from the nematic phase in a strong (ca. 21 kg) magnetic field oriented in the range of 45 ± 15° relative to the normal to the glass plates. This procedure was cycled a few times near the nematic–smectic C transition region. The smectic planes in these samples lie parallel to the glass plates, while the director is in the plane determined by the normal to the plates and the orientation of the field during crystal growth.

Smectic A and B_A crystals of 40,8 and 40,6 doped with PD-Tempone or with CSL were prepared in a similar manner. However, the dimensions of the glass pieces were larger (only X-band experiments were performed for these liquid crystals), the width of the slides ranging between 5 and 7 mm and the length between 10 and 15 mm. The distance between the plates was monitored by teflon or glass spacers to range between 100 and 800 μm. The sandwich samples were placed within a protecting thin-walled Pyrex tube.

For samples containing PD-Tempone, a deoxygenating procedure was developed. The Pyrex tube was first degassed on a vacuum line, and then N_2 was added. The assembly was then introduced into an oil bath heated to a temperature slightly above the smectic A–nematic phase transition and left at that temperature for 10–24 h, with the length of time depending upon the thickness of the sample. During that time the oxygen which was dissolved in the liquid crystal was replaced by N_2 by slow diffusion.

The deoxygenation procedure was considered to be completed and the crystal alignment appropriate when the hyperfine line widths (for H parallel to the director) in our plate samples and in the analogous tube samples of Lin and Freed[6] were virtually identical at the same temperatures.

The smectic A and B_A crystals were obtained by slowly lowering the temperature from the nematic phase to smectic A in the presence of an external field of 13.5 kG oriented normal to the glass surfaces. This procedure was cycled a few times near the nematic–smectic A phase transition region.

Assuming that good homeotropic alignment has been achieved, one expects the smectic layers to be parallel to the glass plates and the smectic A and B_A directors to be perpendicular to the glass plates. Then, complete extinction of light when the smectic crystals were viewed under a microscope between two crossed polarizers, with the slits within the smectic planes, was considered to be indicative of nearly perfect alignment. Such samples were completely transparent; thus visual examination was found to be reliable in estimating the quality of the homeotropic alignment. Then the ESR spectra were used to obtain a more quantitative estimate of the extent of alignment. Both relative and absolute changes in the various spectral features were found to be reproducible as a function of sample preparation (samples with occasional broad lines were discarded). Further discussion on the quality of the smectic crystals will be presented in the following.

B. ESR Spectrometer. The ESR measurements were performed on a Varian E-12 spectrometer by using 10-kHz

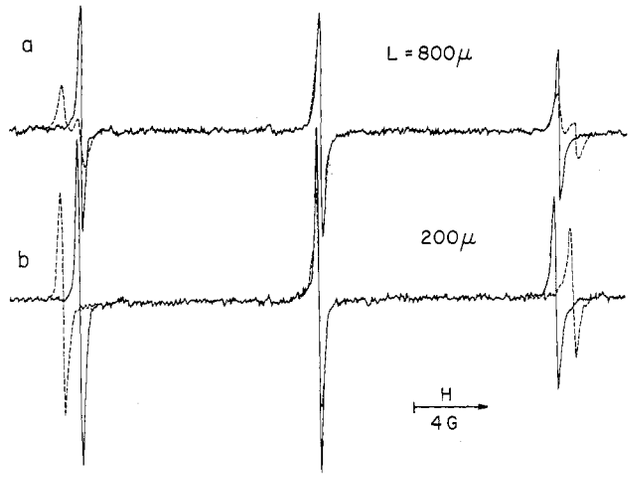

Figure 1. ESR spectra of 5×10^{-4} M PD-Tempone in smectic A crystals for 40,8 at 63.8 °C contained between glass plates, for the external field normal to the glass surfaces, i.e., $\alpha = 0°$ (—) and tilted at 45° relative to the plate normal, i.e., $\alpha = 45°$ (- - -), for a sample thickness of (a) 800 and (b) 200 μm.

field modulation for PD-Tempone and 100-kHz field modulation for CSL. The temperature in the active region of the cavity was controlled by a Varian E-257 variable-temperature control unit to a long-term stability of ±0.3 °C. The temperature of the sample was controlled by using a copper–constantan thermocouple placed just above the sample. By using extra pole caps, we could raise the magnetic field to 21 kG.

III. Results and Discussion

A. Study of Sample Morphology. We have already noted that in order to obtain orientation-dependent spectra, free from effects of inhomogeneous broadening, one should take great care with the morphology of the sample. It was found in our ESR studies on smectic phases with cylindrical tube sample holders that the extent of static inhomogeneous broadening depends upon the size (and shape) of the sample holder.[6] It was pointed out in that work that a proper study of such effects should be performed by using samples oriented between plates. We now wish to discuss our preliminary results of this type of experiment (as noted in the previous section, the plating-out of the PD-Tempone in the smectic phases in a short time, ca. 1–2 h, prevented us from more detailed studies).

We present in Figure 1, ESR spectra obtained from PD-Tempone in the smectic A phase of 40,8 at 63.8 °C from plate samples with $L = 800$ and 200 μm, respectively (where L is the sample thickness) for the external field H perpendicular to the glass plates (i.e., $\alpha = 0°$, giving the solid lines in Figure 1) and also tilted at $\alpha = 45°$ relative to n (where n is the normal to the glass surfaces). The line width of the hyperfine components at $\alpha = 0°$ for both samples is identical with that observed in the tube samples[6] at the same temperature. Also, the hyperfine splittings for $\alpha = 0°$ and the splitting of the 200-μm sample for $\alpha = 45°$ are identical with the corresponding hyperfine splittings in the tubes at the same temperature (see Figure 4a of ref 6). At $\alpha = 45°$, a well-defined triplet is observed for the 200-μm sample, whereas a distribution of sites with peaks for orientations parallel to the field as well as tilted by about 45° to the field is observed for the 800-μm sample, but this latter effect is reversible by reorienting the sample to $\alpha = 0°$.

We interpret these observations in terms of elastic layer deformations due to undulations induced by the tilted magnetic field; i.e., the smectic layers distort by undulatory modes to minimize the magnetic free energy (due to the diamagnetic anisotropy of the smectic molecules) while keeping the layer spacings very nearly constant as is consistent with the strong smectic aligning forces. These undulatory modes are suppressed by strong homeotropic alignment by the plates, and previous theories have shown that (1) the magnetic fields needed for inducing distortions are very large (ca. 50 kG) or else centimeter thick samples are needed, and (2) these distortions should be very weak. Our experimental results showing large distortions for the 800-μm sample are thus in sharp conflict with previous theory. We have reexamined the theory with particular emphasis on the role of finite anchoring forces instead of the usual assumption of perfect homeotropic anchoring in the smectic phase. Our analysis is outlined in Appendix A, where we show that the strength of the anchoring for our simple model depends upon the dimensionless ratio: $(\pi/2)[K_N/(\bar{B}K_1)^{1/2}]$ where K_N is the force constant on the surface (in units of force/distance) that induces the homeotropic alignment while $\bar{B}$ is the smectic layering force (in units of force per unit area) and K_1 is the splay elastic constant (in units of force). Thus the strength of the anchoring is to be compared relative to $(\bar{B}K_1)^{1/2}$ which is very large [because of $\bar{B}$] and this strongly suggests that a condition of weak anchoring actually applies (cf. Appendix A). On the other hand, the strength of anchoring in the nematic phase depends upon the dimensionless ratio $[K_N L/(\pi K_1)]$, and K_1/L is not nearly as strong as $\bar{B}$ (cf. Appendix A). Thus, while a mesogen may exhibit strong anchoring in the nematic phase in the sense that $[K_N L/(\pi K_1)] \gg 1$, it may still not be so strongly anchored in the smectic phase. Thus smectic-phase distortions may be much more easily achieved than predicted for the strong-anchoring limit.

Another possibility is that the small amount of probe (or other impurities) has considerably reduced the strength of $\bar{B}$, but this does not appear too likely in view of the observations that small amounts of probe do not significantly affect the other properties (in particular the phase-transition temperatures) in the nematic, smectic A, or smectic C phases.[1-6]

We thus interpret our observations in terms of undulatory deformations for the 800-μm samples, which imply that for $L = 800$ μm the field of $H = 3300$ G is above the critical field H_c needed to induce distortions, while for $L = 200$ μm, $H_c > 3300$ G, so no significant distortions are observed (although we could not check the line widths carefully before the PD-Tempone plated out in order to see if small distortions were present). Indeed, for samples with $L < 200$ μm, we obtained ESR line shapes identical with those recorded for $L = 200$ μm. As shown in Appendix A, the H_c for undulatory deformations due to a 90° tilt of the external field relative to the undistorted director depends upon $L^{1/2}$; a gradual increase in L in the range $200\ \mu m < L < 800\ \mu m$ would then enable one to determine the critical thickness, L_c (at 3.3 kG), using the ESR spin probe technique.

Since one can still perform measurements suitable for accurate line shape analysis without the use of signal averaging with 200-μm thick samples and a spin-probe concentration as low as 5×10^{-4} M, we are confident that the thin-plate technique is indeed adequate for ESR spin relaxation studies in smectic crystals, even if the monodomain thickness must be further decreased.

Clearly the analysis of anchoring of the tube samples is more complex than plate samples.[6] It is interesting to note, however, that significantly less distortion of the PD-Tem-

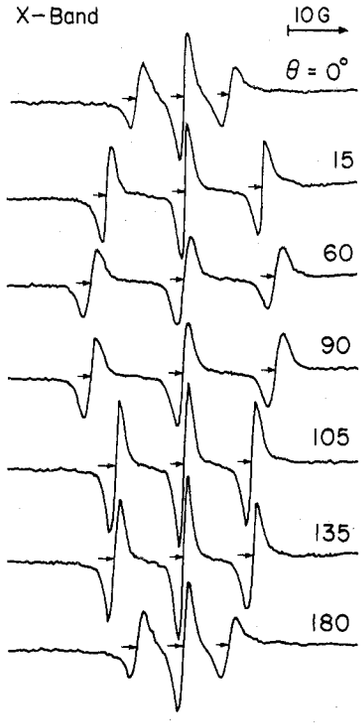

Figure 2. X-band ($H \simeq 3.5$ kG) ESR signals of the cholestane spin probe $\approx 10^{-3}$ M in the smectic C phase (at 80 °C) of HOAB in a glass plate sample of a thickness of approximately 20 μm as a function of the orientation of the magnetic field H relative to the director. The smectic C phase was obtained by cooling the sample from the higher nematic phase with a magnetic field of 21 kG inclined at about 45° to the normal to the plates.

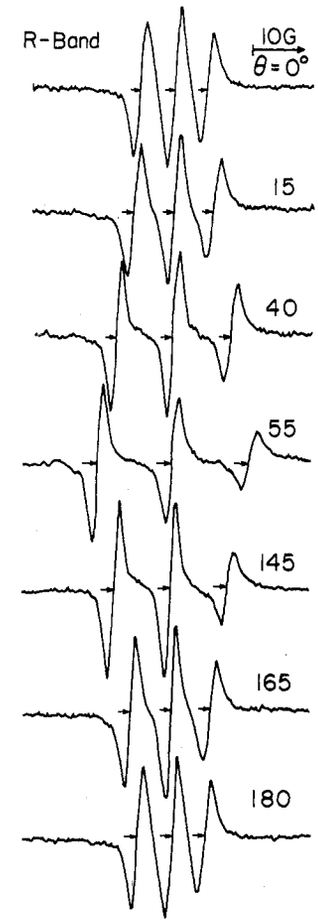

Figure 3. Same as Figure 2 for R band ($H \simeq 12.3$ kG).

pone ESR line shapes is observed from 2×10^3-μm i.d. cylindrical tubes,[6] than from 800-μm plates. This must, at least in part, be due to the fact that the average or "effective" thickness of a well-aligned smectic phase in the tube is much less than its full diameter.

B. ESR Line Shapes. The CSL spectra in HOAB exhibit three well-resolved lines within the nematic phase; the observed hyperfine splitting decreases and the individual lines broaden gradually upon decreasing the temperature. The ratio a_{l0}/a_{0h} (with a_{l0} denoting the separation between the low-field line and the central line and a_{0h} that between the central line and the high-field line) was found to be 1.00 ± 0.03. In the smectic C phase these features are virtually preserved as illustrated in the ESR spectra in Figures 2 and 3. We define for the smectic C spectra a "line shape asymmetry" parameter[6] R to be the ratio between the low-field maximum amplitude to the high-field maximum amplitude and find that at all temperatures and orientations, $0.95 < R < 1.05$, both for the X- and R-band spectra. The small arrows in Figures 2 and 3, denoting the intercept of the baseline with the absorption derivatives, have served to determine R. (We show below that the $\theta = 0°$ spectra at X-band are exceptional and discuss the deviations reflected in these spectra separately; in Figures 2 and 3, θ denotes the angle between the external field H and the smectic C director which is tilted at about 45° relative to the normal to the smectic planes;[13] therefore α, the angle between H and n, the layer normal, is $\alpha = \theta + 45°$.)

For 20-μm thick samples examined at R band, magnetic instabilities resulting in director reorientation occur for field orientations in the range $135° < \theta < 180°$.[14a] (The lower limit of the sample thickness for which good homeotropic alignment can be obtained is 20 μm. This is the average value of the thin film of liquid crystalline material obtained when the nematic liquid is allowed to flow between the plates. To decrease the thickness, pressure must be applied, but the alignment obtained by pressing the plates together was poor, probably due to defect formation.[15a]) At X band (Figure 2), the widths of the various hyperfine components were found to be nearly invariant to changes in the orientation of the magnetic field.

Illustrative ESR spectra of CSL in the various liquid crystalline phases of 40,8 and 40,6 oriented between glass plates from 200-μm thick samples and the magnetic field perpendicular to the glass surfaces are presented in Figures 4 and 5, respectively. We summarize the main spectral features as follows: (a) A well-resolved triplet is observed for all temperatures, from the upper end of the nematic phase to the lower end of the smectic B_A phase. A decrease in the hyperfine splittings and increase in the line widths is observed in the nematic phases, whereas, in the smectic phases, the main effect is a considerable decrease in the observed hyperfine splittings, while the observed line width changes only slightly. (b) The ratio a_{l0}/a_{0h} increased only slightly from 1.00 (1.01) in the nematic phase to 1.04 (1.03) in the smectic B_A phase for 40,8 (40,6).

The experimental values of these spectral features for the liquid crystalline phases of 40,8 and 40,6 are summarized in Table I, A and B.

We proceed by first presenting the analysis of the ESR spectra of CSL in the various nematic phases and show that its motion is similar to that observed previously in phase V.[8] We then focus on the smectic phases where, as will be shown, the ESR spectra reflect new features.

The analysis of all spectra is based on the assumption that the principal axis z' of the ordering tensor is parallel to the magnetic axis y''' and that CSL reorients in the presence of an axially symmetric ordering potential.[8] The magnetic parameters used were those employed in the

TABLE I: Experimental Mean Hyperfine Splittings $\langle a \rangle$ and Ratios a_{1o}/a_{oh} for the Three Hyperfine Components at Various Temperatures

mesophase[d]	temp, °C	$\langle a \rangle$, G[b,c]	a_{1o}/a_{oh}[a]
	A. CSL in 40, 8		
nem	76.8	10.7	1.00
nem	73.0	9.3	1.00
nem	67.7	8.1	1.00
nem	62.4	7.65	1.00
Sm A	59.5	7.65	1.01
Sm A	53.0	6.9	1.02
Sm A	46.9	6.75	1.03
Sm B_A	45.5	6.3	1.04
Sm B_A	30.0	6.0	1.04
Sm B_A	15	5.8	1.04
	B. CSL in 40, 6		
nem	71.0	11.3	1.01
nem	56.6	8.3	1.01
nem	51.0	7.5	1.02
Sm A	49.4	7.5	1.02
Sm A	44.0	6.3	1.03
Sm B_A	42.2	6.3	1.03
Sm B_A	20.0	6.2	1.03

40,8:	Sm B_A	Sm A	nem	iso
	46.1	61.2	77.1	

40,6:	Sm B_A	Sm A	nem	iso
	43.0	50.0	72.0	

[a] a_{1o} and a_{oh} denote the separations between the low-field and the central hyperfine component and that between the central line and the high-field component, respectively; the accuracy in a_{1o}/a_{oh} is ±0.01. [b] $\langle a \rangle$ is defined as $^1/_2(a_{1o} + a_{oh})$; the accuracy in the value of $\langle a \rangle$ is ±0.15 G. [c] The isotropic value a_N for 40,6 was found to decrease from 14.70 G at 72.5 °C (above the nematic isotropic phase transition) to 14.63 at 83.6 °C. [d] Transition temperatures for approximately 10^{-3} M CSL-doped liquid crystal.

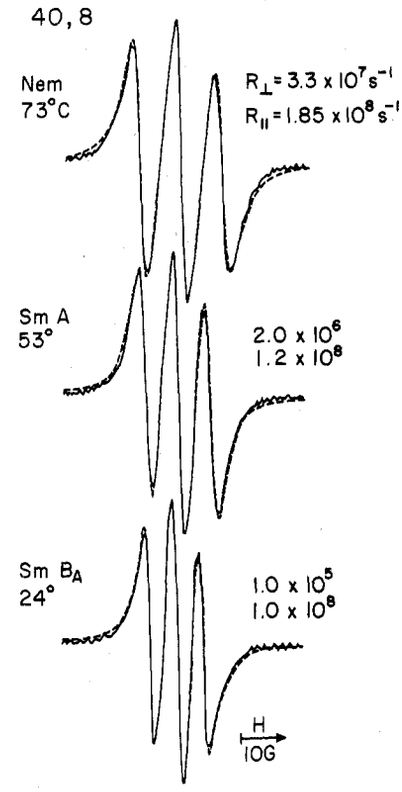

Figure 4. ESR spectra of CSL (≈10^{-3} M) in the various mesophases of 40,8 contained between glass plates with $L \simeq 200$ μm for the external field parallel to the director ($\theta = 0°$), with the monodomain smectic crystals obtained as described in the Experimental Section (—). The computed spectra (- - -) were obtained with (a) $\lambda = 4.1$, $A' = 2.2$ G, $R_\parallel = 1.85 \times 10^8$ s^{-1}, and $R_\perp = 3.3 \times 10^7$ s^{-1} for the nematic spectrum (73 °C); (b) $\lambda = 9.0$, $A' = 2.3$ G, $R_\parallel = 1.2 \times 10^8$ s^{-1}, and $R_\perp = 2.0 \times 10^6$ s^{-1} for the smectic A spectrum (53 °C); and (c) $\lambda = 13.0$, $A' = 2.4$ G, $R_\parallel = 1.0 \times 10^8$ s^{-1}, and $R_\perp = 1.0 \times 10^5$ s^{-1} for the smectic B_A spectrum.

analysis of CSL in phase V.[8] (We encountered difficulties in recording the rigid limit spectra in the plate samples due to the "plating out" of CSL at low temperatures. Therefore, we used tube samples to record the rigid-limit spectra, and we found them to be very similar to the powder spectrum obtained for CSL in phase V.[8] Also, the isotropic values of a_N and g in HOAB, 40,8, and 40,6 were found to be very close to those observed in phase V.)

C. CSL in the Nematic Phases of HOAB, 40,8, and 40,6. 1. HOAB. The line widths were measured as a function of temperature and spectrometer frequency (9.5 GHz at X band and 35 GHz at R band). In all cases the spectra were motionally narrowed ones. We found that the relative changes in the line width as a function of temperatures are larger at R band than at X band.

The isotropic phase of HOAB could not be examined experimentally with the commercial R-band cavity of the E-12 Varian ESR spectrometer which cannot be heated safely above about 120 °C. The temperature-dependent R-band spectra and the rather insensitive (to temperature changes) X-band spectra were, however, available for analysis. The approach adopted was to perform an overall best-fit analysis of all the spectra with τ_R, N, E_a (the activation energy for τ_R), and A' (the intrinsic line width) as the free parameters utilizing the theoretical approach of Freed and co-workers[6,8,10,11] for a rotational diffusion model of reorientation. The order parameter $\langle D_{00}^2 \rangle$ was obtained from the splittings[6] and then converted to the dimensionless potential parameter.[11,21]

TABLE II: Dynamic Rates, λ, and A' Values for CSL in the Nematic and Smectic C Phases of HOAB at Different Temperatures

temp, °C	mesophase	λ[a]	$\langle D_{00}^2 \rangle$	A', G	apparent $R_\parallel$ (s^{-1}) × 10^{-9}	apparent $R_\perp$ (s^{-1}) × 10^{-9}	apparent N
119.7	nem	6.1	0.72	2.1 ± 0.1	13.0 ± 1.0	2.4 ± 0.08	5.4
90.7	nem	9.0	0.82	2.2 ± 0.1	5.4 ± 0.3	1.0 ± 0.06	5.4
89.5	Sm C	9.5	0.83	2.3 ± 0.1	4.0 ± 0.2	0.35 ± 0.01	11.4
80.0	Sm C	11.0	0.86	2.3 ± 0.1	3.6 ± 0.2	0.25 ± 0.01	14.4
71.8	Sm C	≈12.5	0.88	2.3 ± 0.1	3.2 ± 0.2	0.16 ± 0.02	20

HOAB:[b]	solid	Sm C	nem	iso
	71.8	90.1	120	

[a] The values of $\langle D_{00}^2 \rangle$ have been measured directly from the spectra; the corresponding values of λ were obtained with a $\langle D_{00}^2 \rangle$ vs. λ calibration curve computed by Polnaszek.[21] [b] Transition temperatures for HOAB containing approximately 10^{-3} M CSL.

TABLE III: Dynamic Rates, λ, and A' Values for CSL in 40, 8

A. Nematic Phase

temp, °C	$10^8 R_R$,[a] s^{-1}	$10^7 \bar{R}_R$,[b] s^{-1}	$10^8 R_\parallel$,[b] s^{-1}	$10^7 R_\perp$,[b] s^{-1}	$\lambda^{a,e}$	$\lambda^{b,f}$	$\langle D_{00}^2 \rangle^{c,f}$	A', G
76.8	2.28	8.5	2.08	3.6	2.7	2.7	0.4	2.2 ± 0.1
73.0	2.28	7.9	1.85	3.3	4.2	4.1	0.57	2.2 ± 0.1
67.7	1.72	6.9	1.67	2.9	6.4	6.2	9.725	2.3 ± 0.1
62.4	1.39	5.95	1.39	2.5	6.9	6.5	0.74	2.3 ± 0.1
	(7.2)		(1.72)	(2.65)[d]				

B. Smectic A and B_A Phases

temp, °C	mesophase	λ^g	$\langle D_{00}^2 \rangle^h$	apparent $R_\parallel$ (s^{-1}) × 10^8	apparent $R_\perp$ (s^{-1}) × 10^{-5}	apparent N	A', G
59.5	Sm A	6.5	0.74	1.4 ± 0.15	93 ± 15	15	2.3 ± 0.1
53.0	Sm A	9.0	0.82	1.2 ± 0.2	20 ± 15	60	2.3 ± 0.1
46.9	Sm A	11.0	0.86	1.0 ± 0.3	4 ± 3	250	2.4 ± 0.1
45.5	Sm B_A	11.5	0.87	≈1.0 ± 0.3	$\gtrsim 10^5$	≈1000	2.4 ± 0.1
30-15	Sm B_A	⩾13.0	⩾0.89	≈1.0 ± 0.3	$\gtrsim 10^5$	≈1000	2.4 ± 0.1

[a] The values of R_R and λ for a strong-collision model were derived respectively from Figures 4 and 2 of ref 2a, with $R_R \equiv {}^1/_6 \tau_R$. [b] Results obtained from a complete (slow-motional) theory $\bar{R}_R \equiv (R_\parallel R_\perp)^{1/2}$. The precision in the correlation times and in λ was estimated to be approximately 15%. [c] The values of $\langle D_{00}^2 \rangle$, corresponding to the best fit λ values, have been calculated as in Table II. [d] Values in parentheses correspond to a best fit line shape computed with the strong-jump model of reorientation.[10,11] [e] From observed splittings. [f] From slow motional analysis. [g] The accuracy in λ decreases from about 10% at the higher temperatures in smectic A to 20% at the lower temperatures. [h] At the lower temperatures (i.e., high ordering) λ has been estimated by extrapolating Polnaszek's λ vs. $\langle D_{00}^2 \rangle$ curve[21] and since this curve levels off at very high ordering, we can only impose a lower limit on this parameter.

TABLE IV: Dynamic Rates, λ, and A' Values for CSL in the Various Liquid Crystalline Phases of 40,6

temp, °C	mesophase	λ	$\langle D_{00}^2 \rangle$	apparent $R_\parallel$ (s^{-1}) × 10^{-8}	apparent $R_\perp$ (s^{-1}) × 10^{-5}	apparent N	A'
71	nem	2.3	0.345	2.1 ± 0.15	420 ± 50	5	2.5 ± 0.1
56.6	nem	5.5	0.68	1.2 ± 0.15	240 ± 30	5	2.5 ± 0.1
51	nem	7.3	0.77	1.0 ± 0.2	200 ± 30	5	2.6 ± 0.1
49.4	Sm A	7.3	0.77	1.0 ± 0.2	56 ± 10	18	2.6 ± 0.1
44.0	Sm A	11.0	0.86	0.85 ± 0.3	2 ± 1	450	2.7 ± 0.15
42.2	Sm B_A	11.0	0.86	0.85 ± 0.3	2 ± 1	450	2.7 ± 0.15
20	Sm B_A	⩾13.0	0.88	≈0.85 ± 0.3	$\gtrsim 1$	≈850	2.7 ± 0.15

We found that, upon decreasing the temperature, τ_R increases gradually from 0.03 to 0.07 ns in the range 119.7–90.7 °C with an E_a of 8.8 ± 1.0 kcal/mol, while λ increases from 6.1 to 9.0. N was found to be 5.4 ± 1. These results are summarized in Table II for the two extreme nematic temperatures studied.

2. 40,8 and 40,6. The slow-tumbling ESR spectra in the nematic phases of 40,8 and 40,6 have been analyzed by complete line shape simulations, and the results are presented in Tables IIIA and IV for 40,8 and 40,6, respectively. Typical experimental spectral features which have assisted us in obtaining these results are summarized in Tables IA and B and illustrative experimental spectra together with best-fit simulated spectra are presented in Figures 4 and 5.

Basically, the behavior of CSL in the nematic phases of HOAB, 40,8, and 40,6 is similar to that observed previously for CSL in phase V.[8] The ordering increases gradually within the phase, although, assuming a linear temperature dependence for $\langle D_{00}^2 \rangle$, we obtain a relatively slower rate of increase in $\langle D_{00}^2 \rangle$ with temperature for 40,8 and 40,6 as compared to HOAB and phase V.[11] The value of N is constant and close to 5 ± 1, as expected from the geometry of the CSL probe.

The activation energy of 8.8 kcal/mol obtained for HOAB compares rather favorably with 10.9 kcal/mol for CSL in phase V[8] and with 9.6 kcal/mol for PD-Tempone in phase V.[11] The rough estimates for E_a obtained for the nematic phases of 40,8 (≈6.0 kcal/mol) and 40,6 (≈7.5 kcal/mol) are somewhat low as compared with the above-mentioned results. These observations are consistent with the dominant dynamic mode of reorientation of CSL as being a simple diffusive reorientation of a partially ordered probe in a uniaxial medium.[11]

For comparative purposes, we have also included in Table IIIa results obtained by Pusnik et al.[2a] for 40,8, using the limiting fast motional theory for the strong collision model of reorientation and an axially symmetric ordering potential $U = \gamma_2 \cos^2 \beta + \gamma_4 \cos^4 \beta$, suggested by Humphries and Luckhurst.[22,23] The predictions for the value of the line width coefficients B and C based on the strong collision model (used by Pusnik et al.[2a]) and on the Brownian diffusion model (used by us) of reorientation are expected to differ for the correlation times prevailing in the nematic phases of 40,8, as estimated from Figure 20 of ref 6. We have therefore performed a complete line shape simulation of the experimental spectrum obtained at 62.4 °C both for Brownian diffusion and for strong jump diffusion and the best fit parameters for these calculated spectra are presented in Table IIIA.

It was found previously for PD-Tempone 40,8 and 40,6[6] that $\tau_R(B)$ is a good index of the correlation time of PD-Tempone, since it is not very sensitive to the particular model. It was shown in this study[6] that anomalous behavior of the spin relaxation is reflected mainly in unusual behavior of $\tau_\parallel$ (for example, decreasing $\tau_\parallel$ values for decreasing temperatures within the same mesophase[6b]), whereas $\tau_\perp$ exhibits normal behavior. Since the absolute values of $\tau_\perp$ were found to compare favorably with $\tau_R(B)$,[6] one would conclude that for PDT $\tau_\perp$ is the correlation time which best reflects the overall molecular reorientation. Our results for CSL in HOAB discussed below are consistent

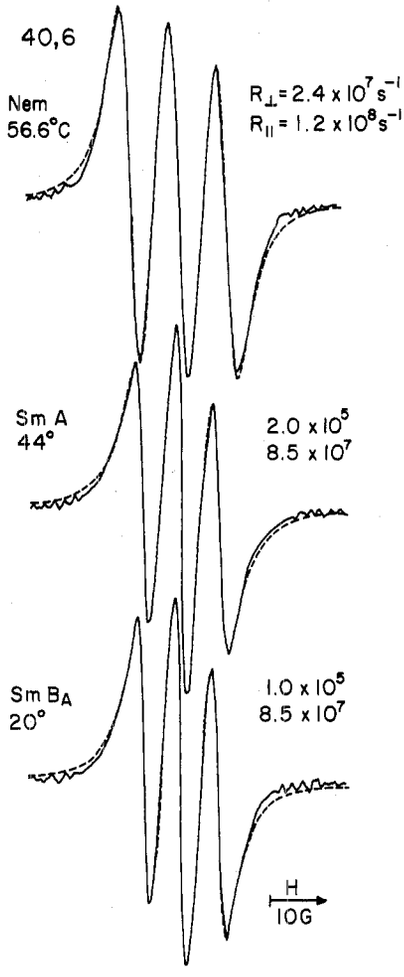

Figure 5. ESR spectra of CSL ($\approx 10^{-3}$ M) in the various mesophases of 40,6 contained between glass plates with $L \simeq 200\ \mu m$ for the external field parallel to the director ($\theta = 0°$), at temperatures as denoted in the figure. The monodomain smectic crystals were obtained as described in the Experimental Section (—). The computed spectra (---) were obtained with (a) $\lambda = 5.5$, $A' = 2.5$ G, $R_\parallel = 1.2 \times 10^8\ s^{-1}$, and $R_\perp = 2.4 \times 10^7\ s^{-1}$ for the nematic spectrum (56.6 °C); (b) $\lambda = 11.0$, $A' = 2.7$ G, $R_\parallel = 8.5 \times 10^7\ s^{-1}$, and $R_\perp = 2.0 \times 10^5\ s^{-1}$ for the smectic A spectrum, and (c) $\lambda = 13.0$, $A' = 2.7$ G, $R_\parallel = 8.5 \times 10^7\ s^{-1}$, and $R_\perp = 1.0 \times 10^5\ s^{-1}$ for the smectic B_A spectrum.

with this, but for CSL in the smectic phases of 40,6 and 40,8 there are very dramatic "apparent" effects on $\tau_\perp$ (see below).

Complete line shape simulation, using the values for $\tau_R(B)$ and λ obtained by Pusnik et al.[2a] by assuming fast motion, resulted in a relatively poor fit to the experimental spectrum at 62.4 °C (discrepancies of the type illustrated in Figure 7 of ref 8 were found), whereas, using slow motional theory, a considerably better fit was obtained with both the strong collision and the rotational diffusion models. (These discrepancies become much worse when the values of Pusnik et al.[2a] for the smectic phases are used.)

We also wish to note at this point that effects of director fluctuations could, in principle, be important at high ordering. We have shown previously for CSL in phase V[8] that the spectral effect is roughly opposite to that from fluctuating torque (i.e., ϵ' corrections, see below), so we cannot rule out the possibility of nearly canceling contributions in these nematic-phase ESR results. Director fluctuations are greatly suppressed in smectic phases; instead one must be concerned with effects of mosaicity as discussed below.

We conclude that a slow motional analysis is likely to be the appropriate approach in analyzing the ESR spectra[8,23] rather than by extending the ordering potential to include the term $\gamma_4 \cos^4 \beta$ and assuming fast motion.

D. CSL in the Smectic Phases of HOAB, 40,8, and 40,6. With complete line shape simulation we found that within the nematic phase of 40,8, A' increases only slightly from (2.2 ± 0.1) G at 76.8 °C to (2.3 ± 0.1) G at 62.4 °C (Table IIIA). In the nematic phase of 40,6, the best fit values were $A' = (2.5 \pm 0.1)$ G at 71 °C and (2.6 ± 0.1) G at 51 °C.

In view of the very small temperature dependence of the ESR spectra in the smectic phases, an accurate estimate for the value of A' is crucial, and we shall therefore elaborate on this to show that it is unlikely that A' increases substantially upon crossing the nematic–smectic transition and upon further decreasing the temperature within the smectic phases.

In principle, an increase in the intrinsic line width A' is expected to occur whenever $\langle a_H \rangle$ or $\langle a_D \rangle$, the superhyperfine electron–proton or electron–deuteron splittings, increase, for example, as a result of increasing ordering. (This is, indeed, the expected trend.[8,24]) Furthermore, as a result of a decrease in the dynamic rates, the anisotropic parts of the superhyperfine tensors, which are normally averaged by the motions, may become incompletely averaged thus leading to further increase in inhomogeneous width.

We found with complete line shape analysis (see below) that $R_\parallel$, the diffusion rate about the main molecular axis, which is the dominant process averaging the hyperfine interaction of the radical with neighboring protons, does not change greatly down to supercooled smectic B_A, implying a relatively small increase in A' throughout the smectic phases, due to inefficient averaging of the superhyperfine interactions. In general, the sensitivity of A' both to changes in ordering and in the dynamic rate was found to be relatively low. Thus, Rao et al.[8] found that, for CSL in phase V, the value of A' increases by only 40% (from 1.75 G at 65 °C to 2.5 G at −26 °C), while the ordering increases substantially and the dynamic rates decrease by more than two orders of magnitude (from 0.9 to 260 ns).

Another possibility to be considered might be a substantial mosaicity in the smectic phases which would result in a considerably larger empirical A' as compared to the nematic phases. This possibility is inconsistent with the results obtained by Lin and Freed[6] for PDT in 40,6 and 40,8 contained in cylindrical tubes. They showed[6] that, although static inhomogeneities exist for the $\theta = 0°$ spectra (where H is parallel to the director as in the present study), these effects are small and probably arise from boundary effects related to the shape of the sample holder. To estimate the extent of mosaicity of a given sample, the "line shape asymmetry parameter" R has been defined for the PDT spectra, and $R \approx 1.00$ has been considered to serve as a criterion for the almost complete suppression of effects of static inhomogeneous broadening.[6] We examined this matter in our study of PDT-doped smectic crystals of 40,8 and 40,6 in plate samples (cf. section A) and found $R = 1.01 \pm 0.03$, so our crystals are at least as good (i.e., free from effects of mosaicity) as the best crystals obtained in the tubes.[6]

Although mosaicity effects on the ESR line widths are expected to be amplified by replacing the weakly ordered PDT probe by the highly ordered CSL probe, there is a much more substantial broadening of the CSL lines due to rather large but unresolved proton superhyperfine splittings such that the relative effects of line broadening due to mosaicity would be expected to be comparable for the two probes. Our observation of $R \approx 1.00$ for PDT is

thus consistent with no more than slight (relative) line width effects due to mosaicity.

For CSL in the smectic C phase of HOAB, the considerations regarding effects of the inhomogeneous line broadening are somewhat different. The samples have been studied at both X and R band. We found that at X band A' is approximately 2.3 G, whereas the average line width is approximately 2.7 G. Then, assuming that A' is mainly determined by the value of $\langle a_H \rangle$, one would expect that any frequency-dependent line broadening, observed upon going from X to R band, is mainly of a homogeneous origin. Note, however, that if crystal mosaicity contributes to the line width at X band, then one would expect this effect to be somewhat larger at R band (due to the increased contribution of the orientation dependent **g** tensor). We present below several arguments showing that, although there is undoubtedly some small misalignment in the smectic C crystals, this effect is *not* very significant.

Lin and Freed[6] showed that the angular dependence of the observed line width should be different for "mosaic" crystals as compared to "perfect" crystals and, furthermore, that the spectral effect of the mosaicity is directly proportional to the extent of ordering. One therefore predicts larger deviations from a "perfect" crystal behavior for CSL than for PDT. Thus, the satisfactory fit of the experimental orientation dependence of the line width at R band to the angular dependence expected assuming good alignment (as discussed below) is considered to reflect the fact that there is a substantial dynamic contribution to the line width.

We have also measured the parameter R in both the X- and R-band spectra and found that $R = 1.00 \pm 0.03$ at R band and 1.00 ± 0.04 at X band, implying little or no crystal mosaicity.[6]

1. HOAB. As we did for the nematic phase of HOAB, we assumed fast motion and rotational diffusion, and we performed a "best-fit" type of analysis, similar to Lin and Freed,[6] for the orientation-dependent spectra at each temperature, with $\langle D_{00}^2 \rangle$ obtained from the experimental splittings, and $R_\parallel$, N, and A' as free parameters. A reasonable fit could only be obtained by allowing N to be somewhat greater than 5, the value expected from the geometry of the CSL probe. The best-fit values of the various parameters are summarized in Table II. The experimentally measured angular dependent line widths of the various hyperfine components (with m denoting the nuclear quantum number) and the theoretical $1/T_2$ vs. θ curves for the 80 °C spectra are presented in Figure 6a. In Figure 6b are plotted the experimental $1/T_2$ values obtained at X band and the theoretical $1/T_2$ vs. θ curves expected with the best fit parameters listed in Table II for 80 °C. The activation energy of 10 ± 1 kcal/mol associated with $R_\perp$ (or with $\tau_R(B)$) is a reasonable one (i.e., a small increase compared to the nematic phase), and we are inclined to offer as our interpretation for the apparent increase in N (or apparent slow decrease in $R_\parallel$) with temperature, not in terms of an anisotropic diffusion model but, as Polnaszek and Freed[11] as well as Lin and Freed[6] did, in terms of a slowly relaxing structure (SRLS) model. That is, in the motional narrowing region one can show[6,11] that an apparent N larger than expected can be equally well analyzed by such a SRLS model. This SRLS model would imply that in the smectic C phase the local "instantaneous" ordering experienced by the CSL probe is somewhat greater than the mean ordering $\langle D_{00}^2 \rangle$, which seems a quite reasonable model for a localized molecular reorientation in the potential field of the oriented but fluctuating liquid crystalline molecules.

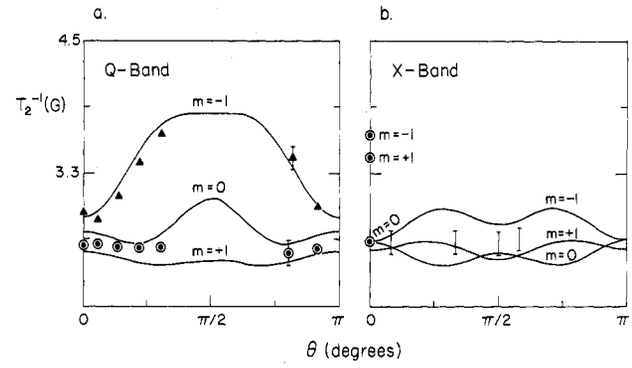

Figure 6. (a) Plot of the experimental line widths $1/T_2$ G^{-1} measured at R band of the various hyperfine components vs. the angle θ between the director and the magnetic field in smectic C at 80 °C: ▲ denote the $m = -1$ component, O correspond to $m = 0$, and ● denote the $m = +1$ component. The full lines were obtained, as outlined in ref 6, assuming that (a) the main (Brownian) ordering axis z' is parallel to the magnetic axis y''' and (b) the ordering potential is axially symmetric, with A' (the intrinsic line width) = 2.3 G, $R_\parallel = 3.6 \times 10^9$ s^{-1}, and $R_\perp = 2.5 \times 10^8$ s^{-1}, $\langle D_{00}^2 \rangle = 0.86$. The principal values of the hyperfine and **g** tensors were $a_z = 33.44$ G, $a_x = a_y = 5.3$ G, $g_z = 2.0021$, $g_x = 2.0089$, and $g_y = 2.0058$ (from ref 8); (b) Experimental line widths measured at X band of the various hyperfine components at 80 °C. The full lines represent the angular dependence of the line widths at 9.3 GHz, calculated with the best fit values of A', $\langle D_{00}^2 \rangle$, $R_\parallel$, and $R_\perp$ obtained from the R-band experiments.

We comment on the following two aspects regarding the analysis illustrated in Figure 6a. Lin and Freed[6] showed that the angular dependence of the line width coefficients B and C (with $(1/T_2)_{obsd} = A + Bm + Cm^2$)[6] should, in principle, differ for Brownian motion and strong jump models of reorientation. In Figure 20 of ref 6 the angular dependence for these two models is presented for $\langle D_{00}^2 \rangle = 0.144$ and 0.557. Among the experimental spectra used in our best fit type of analysis (see Figures 3 and 6a) the main discrepancy is expected to occur for the $\theta = 0°$ spectra; we have estimated its magnitude, assuming that this deviation is linear in $\langle D_{00}^2 \rangle$ and obtained 0.09 G for the B or C terms for $\langle D_{00}^2 \rangle = 0.9$ for the largest value of τ_R in the smectic C phase of HOAB, i.e., $\tau_R = 2.3 \times 10^{-10}$ s at 71.8 °C. Since the accuracy in the experimental line width is ±0.05 G and in the best fit values of A' is approximately ±0.1G, this discrepancy can be ignored, implying that one cannot differentiate between the two models of reorientation.

We have not included in our fast motional analysis the effect of nuclear spin quantization on the line width of the orientation-dependent spectra, which has been studied in detail by Luckhurst and Zannoni.[25] However, from the curves in Figure 2a of ref 25, appropriate for CSL and $\langle D_{00}^2 \rangle = 0.9$, one expects a correction of 0.15–0.2 G for the $\theta = 40°$ spectrum, whereas for all the other values of θ used in our analysis, the correction is less than 0.1 G, and these corrections were not deemed very significant compared with the accuracy of our results.

The ESR experiments outlined above should be extended to other smectic C phases with larger elastic constants for the smectic-C director reorientation, in order to enable one to use the complete rotation pattern at R band, where the orientation-dependent sensitivity is higher.

As mentioned previously, the line widths at X band are practically insensitive both to changes in the temperature and in the orientation of the external field. However, we found consistently that the $m = \pm 1$ components of the $\theta = 0°$ spectrum are considerably wider than the line widths at all the other orientations (see Figures 2 and 6b). The extent of additional line broadening for $\theta = 0°$ cannot be explained by replacing the strong jump model for the

molecular reorientation by rotational diffusion. Using Figure 20 of ref 6, we found that for Brownian diffusion the $\theta = 0°$ lines should be narrower and the $\theta = 90°$ ones broader than observed experimentally. A similar broadening of the X-band lines for $\theta = 0°$ has been observed with a monodomain smectic C crystal of terephthal-bis(butylaniline) TBBA.[13]

Both with HOAB and with TBBA normal behavior was encountered at R band for $\theta = 0°$. It is possible that the effect observed at $\theta = 0°$ at X band is related to deviations from perfect alignment of the smectic C component of the director (i.e., the component in the smectic plane). In a magnetic field its preferential alignment is along the intersection of the smectic plane and the plane defined by the normal to the smectic layer and the magnetic field. As we described in the Experimental Section, in order to obtain a monodomain sample it is necessary to tilt the external field H to an angle close to the smectic C tilt during the preparation. Luckhurst et al.[16] have shown that both the magnitude of H and its orientation relative to the (expected) smectic C director are important in aligning the directors. This is undoubtedly due to the $-H^2 \cos^2 \theta$ dependence of the magnetic free energy term F_{magn} (cf. Appendix A). The $\cos^2 \theta$ term changes only slightly for small variations in θ near $\theta = 0°$, and, for the relatively low value of H at X band, this may well be too small to prevent the decrease in F_{magn} with some misalignment of the smectic-C director. When, however, θ is significantly greater than zero, the $-H^2 \cos^2 \theta$ becomes more important and this should help to improve the alignment of the smectic C director. Misalignment of smectic C directors is most likely avoided simply by using a higher field of about 12.3 kG at R band, so this problem is not manifested in our R-band results.

2. 40,8 and 40,6. For the smectic A and B_A of 40,8 and 40,6 we have only analyzed the $\theta = 0°$ spectra (i.e., the magnetic field parallel to the director) although orientation-dependent spectra may be obtained as well (cf. Figure 7).[26] That the overall appearance of these spectra (cf. Figures 4, 5, and 7) is so similar to the equally spaced fast motional spectra was certainly misleading and resulted in the past to incorrect assignment of the spectra to the fast motional dynamic range. In the smectic phases of 40,6 and 40,8 the ESR spectra are slow motional, and their assignment to this time regime is based on complete line shape simulation.[8,10,11] In general, a slow motional ESR spectrum of a nitroxide radical is characterized by an unresolved pattern of three hyperfine lines.[8,10,11] The resolution to three distinct lines, persisting throughout the smectic phases of 40,8 and 40,6, is due to the particular combination of very high ordering as well as particular aspects of the model. A deeper analysis into the characteristics of these spectra appears warranted, in view of the previous inaccurate analysis of many CSL spectra in thermotropic and lyotropic smectic liquid crystals,[8] which one would expect to display characteristics similar to those of CSL spectra in the smectic A and B_A phases of 40,8 and 40,6. Our approach is to first simulate the spectra using the "basic" model of anisotropic rotational diffusion with a simple orienting potential, and then to reexamine these results in the light of what appears to be more realistic models.[6,8,11]

The various experimentally measured parameters are summarized in Table I, A and B, and illustrative experimental spectra are presented in Figures 4 and 5. The rationale underlying our analysis is based upon the following observations. The relatively small increase in the ratio a_{0l}/a_{0h} upon lowering the temperature from the nematic phase imposes a lower limit on $R_\parallel$; the value of this dynamic rate must be greater than about 10^8 s^{-1} in order to obtain $a_{0l}/a_{0h} \leq 1.04$. The ordering increases considerably upon decreasing the temperature, as evidenced by the decrease in the mean hyperfine splitting $\langle a \rangle \equiv {}^1/_2(a_{0l} + a_{0h})$. We obtain an increase in λ from 2.7 (2.3) at the upper end of the nematic phase to about 13 at the lower end of the smectic B_A phases of 40,8 (40,6). However, the observed line width changes only slightly as the temperature is reduced. Then, to compensate for the narrowing effect of increasing ordering, $R_\perp$ must be decreased substantially, violating the restriction of $R_\parallel/R_\perp \approx 5.0$ for CSL.[8]

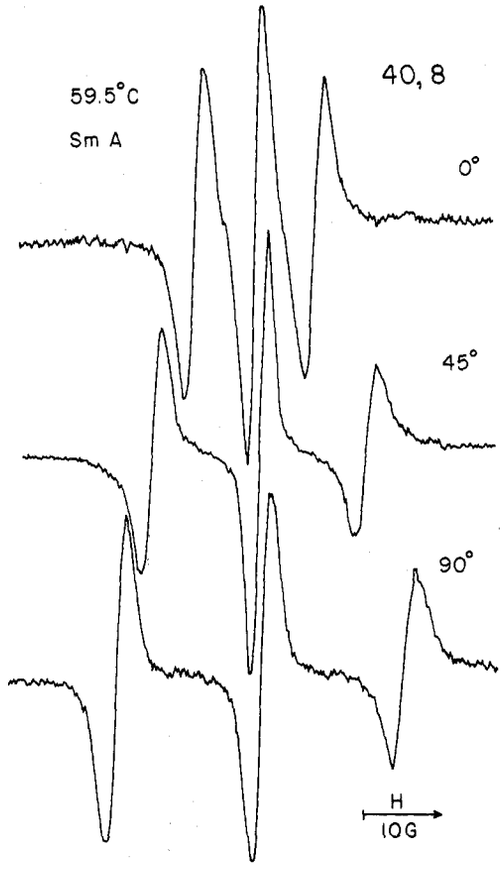

Figure 7. ESR spectra of CSL ($\simeq 10^{-3}$ M) in the smectic A phase of 40,8 for a sample with $L = 200$ μm at various orientations of the external field.

To demonstrate these points, we first tried to simulate the experimental spectrum obtained at the lower end of the smectic A phase of 40,8 at 46.9 °C, with $\lambda = 11.0$, $A' = 2.4$ G, and $N \approx 5.0$ (for $6.0 \leq \lambda \leq 13.0$ the spectra are virtually insensitive to $1 \leq N \leq 7.0$, in agreement with the results obtained for CSL in phase V[8]). The experimental line widths and the *mean* splittings $\langle a \rangle$ could be indeed simulated with $R_\parallel = 1.5 \times 10^7$ s^{-1}; however, the ratio a_{l0}/a_{0h} in the computed spectrum was 1.15 whereas the experimental value of this ratio was 1.03. No further improvement of the *overall* fit could be obtained by varying λ and A'. On the other hand, the overall fit between the theoretical and the experimental spectra throughout the smectic phases of 40,8 and 40,6 was improved substantially by removing the constraint of $N \approx 5.0$.

The "best-fit" theoretical line shapes for several spectra from the various smectic phases of 40,8 and 40,6, calculated with the parameters summarized in Tables IIIB and IV, are illustrated in Figures 4 and 5 together with the corresponding experimental spectra. We found that the apparent $R_\parallel$ decreases in smectic A at rates similar to those observed for weakly ordered probes,[6,8,11] whereas the ap-

parent $R_\perp$ decreases to a much greater extent implying an increase in apparent N up to 1000 (850) within the smectic A phases of 40,8 (40,6).

For the motion in the smectic B phase, we can only say that the results are consistent with $R_\parallel \approx 10^8\ s^{-1}$, $R_\perp \gtrsim 10^5\ s^{-1}$ both for 40,8 and for 40,6 which are the values determined at the lower end of the smectic A phases. Within the smectic B phase the parameter λ is so high that the ESR line shape is practically unaffected by λ (except for the splittings which still decrease with decreasing temperatures), preventing a more accurate determination of λ itself and of the dynamic rates. However, a lower limit on $R_\perp$ is imposed by the relative narrowness of the lines at the lower temperatures in smectic B_A.

The fit between the computed and the experimental spectra in Figures 4 and 5 is very good (as compared to Figure 1 in ref 8). However, we must keep in mind that, by removing the restriction of $N \approx 5$, we have allowed for an additional adjustable parameter and the considerable improvement in curve fitting is expected.

We must now investigate the implications of this improved spectral fitting. At first sight, it would appear that a "very anisotropic diffusion" model would be appropriate for the long CSL molecule in a highly ordered phase which inhibits its reorientation about axes perpendicular to its long axis, while not restricting its reorientation about its long axis (i.e., the z' axis). Thus one would predict $N \gg 1$ for CSL in such phases. This is indeed a reasonable point of view; however, we must discard it for the following reason. The basic diffusion model upon which our simulations are based *automatically* includes the restrictive effects of the surroundings by means of the restoring potential $U = \gamma_2 \cos^2 \beta$ which is *explicitly* included in the diffusion equation.[10] Thus, it should not be necessary to further correct the model by adjusting $R_\perp$. This diffusion coefficient should primarily be a property of the probe molecule itself (and of the "microviscosity" as opposed to the ordering of the medium). We can be more precise by considering the limiting model of diffusion under extremely high ordering potentials. The eigenvalues of the diffusion operator are known[10] and are given by

$$E_{|K-M|}^{\ n} = 2\lambda_2 R_\perp (2n + \nu) + MKR_\perp + K^2(R_\parallel - R_\perp) \quad (1)$$

where $\lambda_2 \equiv -\gamma_2/KT$, $\nu = |K - M|$ and n is an additional quantum number (replacing L) which refers to the angle β between the molecular z' axis and the lab z axis (e.g., $n = 0$ corresponds to the equilibrium distribution in β). Thus the relaxation rate of a nonequilibrium orientation of β is actually *enhanced* by having $\lambda_2 \gg 1$ such that $2\lambda_2 R_\perp$ replaces the $R_\perp$ which is appropriate for the isotropic liquid. This enhancement is expected as a result of the strong restoring torques due to the surroundings. There is another important effect of the high ordering, viz., any nonequilibrium distribution in β (i.e., $n \neq 0$) is highly improbable, and this is explicitly included in the analysis. This latter effect supplies the appropriate restrictive effects of the surrounding walls.

Our fitting procedure given above then corresponds to greatly *reducing* $2\lambda_2 R_\perp$ by greatly lowering $R_\perp$ in order to get good agreement with the spectrum. (Actually λ_2 is not nearly large enough in our results for eq 1 to be quantitatively valid, but it should have qualitative relevance.) This is untenable in the context of the "very anisotropic diffusion" model. Thus we must regard the above fitting procedure as useful empirically but not physically meaningful.

One might then try an anisotropic viscosity model, which would then put the "blame" on anisotropy in the microviscosity of the surroundings.[6,8,10,11] We first note that eq 1 can be rewritten for this case as[10]

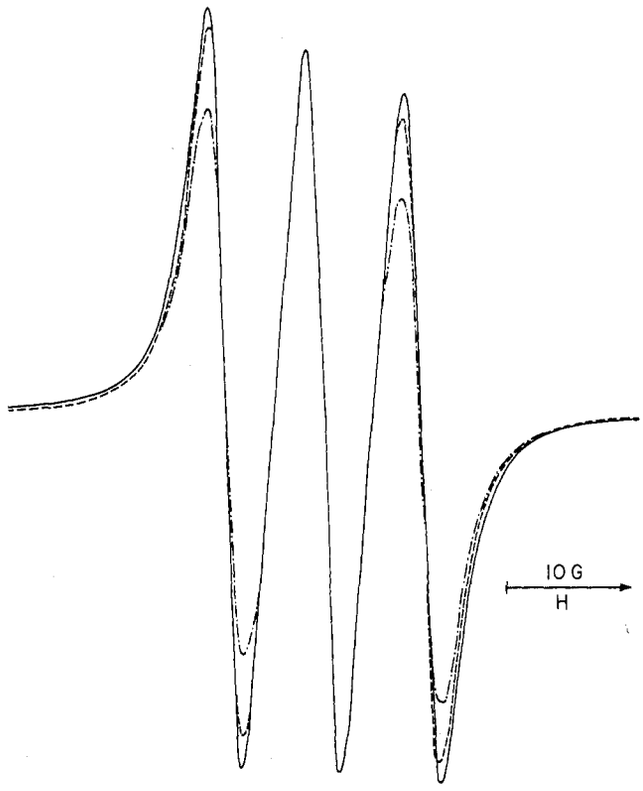

Figure 8. Comparison of the simulated spectra at $R = 1.4 \times 10^8\ s^{-1}$, $\lambda = 6.8$ with different values of ϵ': (—) $\epsilon_{ps}' = \epsilon_s' = 1.0$, $A' = 2.2$ G; (- - -) $\epsilon_{ps}' = 5.0$, $\epsilon_s' = 1.0$, $A' = 2.36$; (-·-·-) $\epsilon_{ps}' = 30.0$, $\epsilon_s' = 1.0$, $A' = 2.4$ G.

$$E_{|K-M|}^{\ n} = 2\lambda_2 \hat{R}_\perp (2n + \nu) + MK\hat{R}_\perp + M^2(\hat{R}_\parallel - \hat{R}_\perp) \quad (2)$$

where $\hat{R}_\parallel$ and $\hat{R}_\perp$ are the parallel and perpendicular components in the lab-director frame. We note that for

$$2\lambda_2 \hat{R}_\perp \gg |R_\parallel - R_\perp| \quad \text{or} \quad |\hat{R}_\parallel - \hat{R}_\perp| \quad (3)$$

the predictions of eq 1 and 2 are identical (with $\hat{R}_\perp \approx R_\perp$), i.e., the probe is so highly ordered that the instantaneous molecular frame (x',y',z') and the lab frame (x,y,z) are virtually the same. Since our results are not consistent with inequality 3 we attempted a fit to the 53.9 °C spectrum of 40,8 by adjusting $\hat{N} \equiv \hat{R}_\parallel/\hat{R}_\perp$, but we could not obtain a reasonable fit.

A more successful point of view, which we have employed for PDT in various liquid crystalline phases,[6,11,28] is to recognize that the instantaneous potential on the probe is not just the mean (or time-averaged) potential U. Instead one should add an additional potential $U'(t)$ with zero mean $\langle U'(t) \rangle$ to represent the instantaneous (but fluctuating) correlations between CSL and the surrounding molecules. This may either be included as a fluctuating torque, which can modify R to make it frequency dependent, and/or it can lead to a slowly fluctuating ordering potential (a SRLS model).[28]

The fluctuating torque model has been introduced into the slow-tumbling formulation in an approximate way,[11] and we have made use of this approach to attempt a fit of our results. This analysis is based upon a correction, which for fast motion would allow us to write for the spectral density $j(\omega) = \tau_R/[1 + \epsilon'\omega^2\tau_R^2]$ where ϵ' is the "non-Brownian" correction, and, in general, we allow secular terms to be characterized by an ϵ_s' and pseudosecular terms by ϵ_{ps}'.

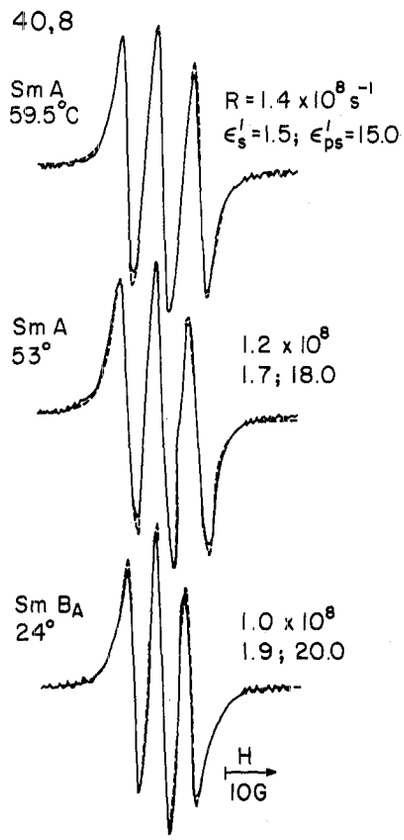

Figure 9. ESR spectra of CSL ($\approx 10^{-3}$ M) in the smectic A and B_A phases of 40,8 contained between glass plates with $L \simeq 200$ μm for the external field parallel to the director ($\theta = 0°$), with the monodomain smectic crystals obtained as described in the Experimental Section (—). The computed spectra (···) were obtained with $A' = 2.3$ and $\lambda = 6.8$ for 59.5 °C, $A' = 2.3$ and $\lambda = 10.0$ for 53 °C, $A' = 2.4$ and $\lambda = 13.0$ for 24 °C, and the corresponding values of R, ϵ_s', and ϵ_{ps}' as denoted in the figure.

We have calculated several line shapes as illustrated in Figure 8 for various values for ϵ_s' and ϵ_{ps}'. The changes in the line shape upon varying ϵ are similar to those illustrated in Figure 5a of ref 8. To test the fluctuating torque model for interpreting the spectra of CSL in the smectic phases of 40,8 and 40,6 we have simulated several experimental spectra for the smectic A and B_A phases of 40,8 as shown in Figure 9. The main point to be emphasized is that the quality of the fits in this figure is comparable to that illustrated in Figure 4, but, instead of an undue increase in N upon lowering the temperature with the "very anisotropic" diffusion model (Figure 4), the series of temperature-dependent spectra could be simulated with $N \approx 1$–5, a small increase in R upon lowering the temperature within the same mesophase and only a small variation of ϵ_s' in the range 1.5–2 and of ϵ_{ps}' in the range 15.0–20.0.

While we would like to compare our experimental results with predictions of a SRLS model, we note that its effects on spin relaxation have only been developed in detail for the motionally narrowed region, where it was found to be consistent with the observed anomalies. Although extensive theoretical work is underway to develop such models and predict their effects on slow-tumbling spectra,[28] it is not yet possible to predict with any accuracy its effects in the present case. The success with which SRLS was able to "explain" fast motional results with apparent anomalously large N values suggests that it may well be successful in "explaining" these slow-motional results on the highly ordered CSL. As noted above, we do favor this model on physical grounds.

IV. Further Discussion and Conclusions

We have found that the motion of CSL in the nematic phases of HOAB, 40,6, and 40,8 is similar in nature to that observed previously in phase V:[8] the motional rates $R_\parallel$ and $R_\perp$ decrease and the orienting potential parameter λ increases gradually upon decreasing the temperature, with a constant anisotropy of about 5 in the axially symmetric diffusion tensor; the activation energies for overall reorientation are in the range of 7–9 kcal/mol. These results are consistent with the motion of CSL consisting mainly of an individual mode with the anisotropy in the diffusion tensor determined by the geometry of the probe molecule.[8]

Upon lowering the temperature to the smectic phases, we have typically found a substantial increase in the *apparent* anisotropy of the diffusion tensor both for fast (in HOAB) and for slow (in 40,6 and 40,8) motion of CSL. We prefer to interpret the spectral anomalies by considering CSL to reorient in a local "cage", the average and instantaneous conformations of which impose restrictions upon the motion of the solute, so that the overall dynamic mode is now determined by the combined effect of individual probe modes and collective solvent modes. This point of view is similar to that summarized recently by Dianoux and Volino[16] based on recent neutron scattering, ^{14}N pure nuclear quadrupole resonance, and ^2H NMR.

More precisely we have reanalyzed and discussed the anomalous relaxation and line shape behavior for CSL in the smectic phases in terms of fluctuating torque and SRLS models, which are two classes of models[28] for the effects of dynamic cooperativity of the reorientation of the CSL molecule with that of the mesogen solvent molecules. In particular, by our detailed simulations we have shown that an approximate fluctuating torque model could adequately account for the slow-motional line shapes without requiring implausibly large increases in anisotropy of the diffusion tensor.

These results and observations with the highly ordered CSL probe are complementary to those obtained with the weakly ordered PD-Tempone probe. In the latter case it was inferred that PD-Tempone is gradually expelled from the rigid core region upon lowering the temperature from the nematic phases of 40,6 and 40,8 into the smectic phases presumably due to increased packing of the mesogen molecules in these more ordered phases. It is such an increased dynamic packing which has been attributed in the present work to increased cooperativity in reorientation of the CSL probe. It was also inferred that the PD-Tempone experiences a substantial contribution from the SRLS mechanism in a somewhat lower ordered region of the smectic layer, but again this is consistent with the results for CSL.

We would like to emphasize two aspects of the present study on slow motion in the smectic phases. On one hand, due to the relatively small variation of some of the spectral features (such as the observed line width) as a function of temperature and due to the intrinsic low sensitivity to the dynamics of the ESR spectra in this region of very high ordering and slow motion, our results are rather imprecise, the limits of accuracy in the various parameters being as high as ±50%. On the other hand, the implications of the small variation, and the restrictions imposed by those spectral features which do vary as a function of temperature (such as, for example, the hyperfine splittings) do lead to reasonably reliable conclusions about the motion of the rigid CSL probe in the highly structured smectic phases.

It is our hope to improve on these results by increasing spectral resolution with the use of deuterated CSL and other deuterated probes and by studying further the fre-

quency dependences as well as the angular dependences of these spectra in the highly ordered phases. We believe such experiments should be sufficient motivation for developing and improving the theoretical models for cooperative rotational reorientation and their effects on ESR line shapes.

Finally, we would like to emphasize again the importance of proper sample preparation in the form of thin and strongly anchored monodomain smectic crystals having high critical fields with respect to layer deformations, whenever angular-dependent measurements in smectic phases are performed.

Acknowledgment. This work was supported by NSF Grant DMR-77-17510.

Appendix A. Magnetic-Field-Induced Instabilities in the Smectic A Phase

The theory due to Hurault for transitions induced by a magnetic field on a smectic A in a homeotropic alignment between two glass plates has been summarized by de Gennes.[29] This analysis was based on the assumption of strong homeotropic alignment at the glass plates, and it did not include nonlinear terms to explicitly estimate the magnitude of the distortion.

We generalize the description here to allow for less than perfect anchoring, and we introduce nonlinear terms appropriate for small magnetic-field-induced distortions. We write the free-energy density of the bulk as[29-31]

$$F^{s}_{vol} = \frac{1}{2}\bar{B}\left[\frac{\partial u}{\partial z} - \frac{1}{2}\left\{\left(\frac{\partial u}{\partial x}\right)^2 + \left(\frac{\partial u}{\partial y}\right)^2\right\}\right]^2 + \frac{K_1}{2}\left(\frac{\partial^2 u}{\partial x^2} + \frac{\partial^2 u}{\partial y^2}\right)^2 - \frac{1}{2}\chi_a H_0^2 \cos^2 \psi_{\bar{r}} \quad \text{(A1)}$$

Equation A1 includes only those distortion energies of importance with respect to the smectic alignment. The first term in eq A1 represents the smectic layering free energy with $\bar{B}$ the elastic constant for compression of the layers, and $u(\vec{r})$ measures the displacement of the smectic layers from equilibrium at point $\vec{r}$. The equilibrium is taken such that the smectic layers are parallel to the aligning plates, and the z axis is normal to them, while the magnetic field H_0 is in the x–z plane. We also note that this first term is corrected for tilting through a small angle, e.g., $\partial u/\partial x$. [In the case of large distortions, this correction is insufficient and a more general formulation is required, which, however, would considerably complicate the analysis.[31]] The second term in eq A1 is the free energy term from splay distortion with K_1 the associated elastic constant. The last term in eq A1 is the magnetic free energy, where χ_a is the anisotropy in the diamagnetic susceptibility and $\cos \psi_{\bar{r}} \equiv \hat{n}(\vec{r})\cdot\vec{H}_0$, where $\hat{n}(\vec{r})$ is the nematic director at $\vec{r}$, and is everywhere normal to the smectic layers. This means that, at equilibrium in the absence of H_0, $\hat{n}$ is parallel to z. The effect of a nonzero H_0 in the x–z plane is to introduce distortions (assumed small in this analysis) characterized by $n_x = -\partial u/\partial x \ll 1$ (and $n_y = -\partial u/\partial y \ll 1$). If α is the angle of tilt between H_0 and the z axis, then $F_{magn} = -{}^1/_2\chi_a H_0^2[n_z \cos \alpha + n_x \sin \alpha]^2$. We shall treat the simple case of H_0 along the x-axis below.

The surfaces of the aligning plates are at $z = 0$ and L, and in the absence of better knowledge of surface alignment of smectics we represent the surface free energy favoring the homeotropic alignment by either of two forms

$$F^{s}_{surf} = {}^1/_2K_N(n_x^2 + n_y^2) \quad \text{(A2a)}$$

or

$$F^{s}_{surf} = {}^1/_2K_S\left(\frac{\partial n_x}{\partial x} + \frac{\partial n_y}{\partial y}\right)^2 \qquad z = 0, L \quad \text{(A2b)}$$

(where F_{surf} is in units of energy per unit area). Equation A2a is similar in form to what is usually used to discuss anchoring in the nematic phase,[32] while eq A2b is a form similar to the splay term in eq A1. In the limit $K_N(K_S) \to \infty$ one recovers strong anchoring for which $\hat{n}$ ($z = 0$) and $\hat{n}$ ($z = L$) are perfectly aligned along the normal to the plates. Thus, either form is sufficient to span the weak to strong anchoring limits for the nematic director, as will be seen below.

Normally, one expands $u(\vec{r})$ in Fourier components, but we shall essentially consider only the lowest component(s), which will be the one(s) most easily deformed.[29-31] That is, we shall let

$$u(x,z) = u_0(z) \cos kx \quad \text{(A3)}$$

where the wave vector k is at present arbitrary, but we shall later seek the optimum value for deformation.

When we substitute eq A3 into eq A1 and A2 we obtain

$$F^{s}_{vol} = {}^1/_2\bar{B}\left[\left(\frac{\partial u_0}{\partial z}\right)\cos kx - {}^1/_2u_0^2(z)k^2 \sin^2 kx\right]^2 + {}^1/_2K_1k^4u_0^2(z)\cos^2 kx - {}^1/_2\chi_a H_0^2k^2u_0^2(z)\sin^2 kx \quad \text{(A4)}$$

$$F^{s}_{surf} = {}^1/_2K_Nk^2u_0^2(z)]_{0,L}\sin^2 kx \quad \text{(A5a)}$$

or

$$F^{s}_{surf} = {}^1/_2K_Sk^4u_0^2(z)]_{0,L}\cos^2 kx \quad \text{(A5b)}$$

We now seek to minimize the total free energy

$$F^{s}_{T} \equiv \int_0^L dz \int dx\, F^{s}_{vol} + \int dx\, F^{s}_{surf} \quad \text{(A6)}$$

with respect to the functional $u_0(z)$ according to the variational principle. But first we perform the integrations over x by replacing in eq A4, A5, and A6 the functions $\cos^2 kx$, $\sin^4 kx$, and $\cos kx \sin^2 kx$ by their averages of 1/2, 3/8, and zero, respectively. We then obtain from the Euler Lagrange equation (i.e., from $\partial F_{vol}/\partial u_0 - (d/dz)[\partial F_{vol}/\partial(\partial u_0/\partial z)] = 0$):

$$-\bar{B}\left[\frac{d^2u_0}{dz^2} - {}^3/_8u_0^3k^4\right] + (K_1k^2 - \chi_a H_0^2)k^2u_0(z) = 0 \quad \text{(A7)}$$

Equation A7 is subject to the boundary conditions [from

$$\left(\frac{\partial F_{vol}}{\partial\left(\frac{\partial u_0}{\partial z}\right)} \mp \frac{\partial F_{surf}\,(z = 0,L)}{\partial u_0}\right)\Bigg|_{z=0,L} = 0$$

with the $-(+)$ sign for $z = 0(L)$]:

$$\left(\bar{B}\frac{du_0}{dz} \mp K_Nk^2u_0(z)\right)\Bigg|_{z=0,L} = 0 \quad \text{(A8a)}$$

or the equivalent form from eq A5b. We now rewrite eq A7 as

$$\frac{d^2u_0}{dz^2} + \omega^2u_0 + \mu u_0^3 = 0 \quad \text{(A9)}$$

where

$$\omega^2 \equiv \bar{B}^{-1}(\chi_a H_0^2 - K_1k^2)k^2 \quad \text{(A10a)}$$

$$\mu \equiv -{}^3/_8k^4 \quad \text{(A10b)}$$

with boundary conditions

$$du_0/dz = \gamma u_0 \quad \text{at} \quad z = 0 \tag{A11a}$$

$$du_0/dz = -\gamma u_0 \quad \text{at} \quad z = L \tag{A11b}$$

$$\gamma \equiv K_N k^2/\bar{B} \quad (\text{or} \equiv K_S k^4/\bar{B}) \tag{A11c}$$

When the distortion is small, the term μu_0^3 in eq A9 will be small, so we can use the method of Krylov and Bogoliubov[34] to obtain an approximate solution of this nonlinear differential equation. One obtains as the solution to eq A9

$$u_0 \simeq A \sin [\omega z(1 + \alpha) + \varphi_0] \tag{A12}$$

which is a good approximation if

$$\left|\alpha \equiv \frac{3\mu A^2}{8\omega^2}\right| \ll 1 \tag{A13}$$

The amplitude A and the phase φ_0 may be determined by the boundary conditions eq A11. We note first that for $\gamma \to \infty$ we obtain the strong anchoring condition

$$u_0(0) = u_0(L) = 0 \tag{A14a}$$

while for $\gamma \to 0$ we have the free surface boundary condition

$$\left.\frac{du_0}{dz}\right|_{z=0,L} = 0 \tag{A14b}$$

The general relations for $\alpha \propto A^2$ and φ_0 are

$$\tan [\omega L(1 + \alpha)] = \frac{2\omega(1 + \alpha)\gamma}{[\omega(1 + \alpha)]^2 - \gamma^2} \tag{A15a}$$

$$\tan \varphi_0 = \omega(1 + \alpha)\gamma^{-1} \tag{A15b}$$

It also follows from eq A9 and its approximate solution eq A12 that $\omega^2 > 0$ for allowed solutions (e.g., for $\mu \approx 0$, the case of $\omega^2 < 0$ would lead to a solution of form $u_0 = Ae^{-z/l} + Be^{z/l}$, $l^{-1} \equiv i\omega$ which cannot satisfy the boundary conditions, eq A11, except for $l^{-1} = 0$).

(1) Perfect Anchoring Limit. We now consider the strong anchoring limit for which $\gamma = \infty$. Then eq A15a yields

$$\omega L(1 + \alpha) = n\pi \qquad n = 1, 2, 3, \ldots \tag{A16a}$$

while eq A15b gives

$$\varphi_0 = 0 \tag{A16b}$$

Except for $\alpha \neq 0$ this result is identical with that already given for strong anchoring.[29] One has from eq A16a, using eq A13 that

$$\omega \approx \frac{n\pi}{L}\left[1 + \left(\frac{3}{8}\right)^2 \frac{A^2}{\omega^2} k^4\right] \tag{A17}$$

which is a relation for A^2 as a function of k^2, and from which the critical field H_c may be determined. If we first set $A \approx 0$, then eq A17 yields

$$k^2 = \frac{\chi_a H_0^2}{2K_1} \pm (\chi_a^2 H_0^4 - 4K_1\pi^2 n^2 \bar{B}/L^2)^{1/2}/2K_1 \tag{A18a}$$

$$n = 1, 2, 3, 4$$

yielding

$$\chi_a H_c^2 = 2\pi K_1^{1/2} \bar{B}^{1/2}/L \qquad n = 1 \tag{A18b}$$

$$k_c^2 = \frac{\chi_a H_c^2}{2K_1} \tag{A18c}$$

the result given previously for H_c in this limiting case.[29]

Note that eq A18c required in order that k, the wave vector, be real is a somewhat stronger requirement on k than $\omega^2 > 0$ from eq A10a (and preserves the validity of the solution eq A12).

We can obtain an approximate solution to eq A17 by letting $\omega^2 \approx (n\pi/L)^2$ in the denominator of the term in A^2 and then solving the resulting equation for k^2. One obtains a form very similar to eq A18a; it is just necessary to replace $K_1 \to \hat{K}_1 \equiv K_1 + {}^1/_2({}^3/_4)^2 A^2 \bar{B}$, and the approximate validity of this solution just requires that $\hat{K}_1/K_1 \equiv 1 + \epsilon$ where $0 < \epsilon \ll 1$. Then we get $H_{c,new}^2/H_{c,old}^2 \approx (1 + {}^1/_2\epsilon)$ and $K_{c,new}^2/K_{c,old}^2 \approx (1 - {}^1/_2\epsilon)$; i.e., for nonzero ϵ (or A^2) a higher H_c^2 but lower k_c^2 is required. [The subscript old refers to the values given in eq A18, while the subscript new refers to the values associated with a finite ϵ (or A^2).]

(2) Strong Anchoring. We now study the results for γ large but not infinite. Then eq A15a,b give

$$\omega L(1 + \alpha)\left(1 + \frac{2}{\gamma L}\right) \approx n\pi \qquad n = 1, 2, 3, \ldots \tag{A19a}$$

$$\varphi_0 \approx \omega/(1 + \alpha)\gamma^{-1} \tag{A19b}$$

We now solve eq A19a by the approximation scheme just utilized (i.e., by letting $\omega^2 \approx (n\pi/L)^2$ in α and letting $\hat{L} \equiv L + 2/\gamma$). Now we obtain eq A18 but with $K_1 \to \hat{K}_1$ and $L \to \hat{L}$.

Since $\hat{L}$ is a function of k^2 (cf. eq A11c), we can approximate it in the region of $\chi_a H_c^2$ and k_c^2 by first using the solution for these values obtained in section 1 and inserting into the definition of $\hat{L}$ to obtain

$$\hat{L} \approx L(1 + \delta_i) \quad \text{for } H_0^2 \sim H_c^2 \tag{A20a}$$

with

$$\delta_N \equiv \frac{2}{\pi}\frac{(\bar{B}\hat{K}_1)^{1/2}}{K_N} \quad \text{or} \quad \delta_S = \frac{2}{\pi^2}\frac{\hat{K}_1}{K_S}L \tag{A20b}$$

This apparent increase in L due to less than perfect anchoring given by eq A20 justifies the point of view taken previously by Lin and Freed[6] for this case of strong anchoring. In particular we obtain from this approximate analysis

$$\chi_a H_{c,new}^2 \approx \chi_a H_{c,old}^2 \frac{(1 + {}^1/_2\epsilon)}{(1 + \delta_i)} \tag{A21a}$$

$$\varphi_0 \approx \frac{\pi}{2}\delta_i(1 + \delta_i) \tag{A21b}$$

The nonzero phase φ_0 yields a nonzero value of $u(L) = u(0) = A \sin \varphi_0 \simeq A\varphi_0$, so that $n_x(x,0) \approx n_x(x,L) \approx k_c A\varphi_0 \sin k_c x$; i.e., a director tilt even at the surfaces.

We now wish to compare the dimensionless anchoring parameter δ_N and δ_S. The latter is somewhat similar to the parameter $\beta^{-1} = \pi K_1/(LK_N)$ for nematics,[32] so it does not depend at all on the strong smectic force constant $\bar{B}$. We prefer the form of δ_N, because (1) it is based on eq A2a which appears to apply reasonably well to nematics and yet (2) it includes a dependence upon $\bar{B}$, which appears quite sensible physically. That is, the perpendicular magnetic field attempts to reorient the smectic layers in the bulk, and it is the large smectic layering forces which transmit this to the surface molecules, i.e., (the $\bar{B}$ as well as the K_1 terms) "transmit" the competition between surface alignment and magnetic alignment.

It is possible to estimate δ_N from the following typical values:[29] $\bar{B} \sim 2 \times 10^7$ dyn/cm^2, $K_1 \sim 10^{-6}$ dyn, $\chi_a \sim 10^{-7}$ cgs, with K_N ranging from 10^{-2}–10^{-4} dyn/cm,[35] depending upon surface preparation (we would estimate the larger

values of K_N for our work). One obtains $\delta_N \sim 3 \times 10^2$–$3 \times 10^4$ or hardly a small parameter! Thus, on the basis of order of magnitude estimates it appears that it is incorrect to explain our experiments with the limiting case of strong anchoring.

(3) *Weak Anchoring.* In the general case we must solve eq A15a numerically. This is best done by rewriting it as $\tan(ay) = 2y(y^2 - 1)^{-1}$ with $y \equiv \omega(1 + \alpha)\gamma^{-1}$ and $a \equiv L\gamma$. Or alternatively we have

$$\tan^{-1}\frac{2y}{y^2 - 1} = ay - n\pi \qquad n = 0, 1, 2, \ldots \tag{A22}$$

The numerical solutions of eq A22 show that for $n = 1$

$$ay = \omega(1 + \alpha)L \approx \pi\ (\pm 15\%) \tag{A23}$$

over most of the range of a (except for $a \approx 2$–10 where there are typically two roots of the order of 50% larger and smaller than eq A23). Thus the perfect anchoring result of eq A18b leading to $H_c \approx 60$ kG[29] is not drastically altered, except that φ_0 ranges continuously from $\pi/2$ for very small a to zero for very large a.

However, we have found that for $a \lesssim 1$ and $n = 0$ there are acceptable solutions to eq A22 (aside from the trivial $y = 0$). They are well approximated (even for $a \sim 1$) by the approximate form from eq A22

$$y \approx (2/a)^{1/2} \qquad a \lesssim 1 \tag{A24a}$$

Equation A24a may be rewritten as

$$k^2K_1 \approx \chi_a H_0^2 - 2K_N(1 + \alpha)^{-2}L^{-1} \quad a \lesssim 1 \tag{A24b}$$

from which the requirement $k^2 > 0$ leads to

$$(1 + \alpha)^2\chi_a^2 H_c^2 > 2K_N L^{-1} \tag{A24c}$$

The above typical values (and $L \sim 10^3$ μm) then lead to $H_c \approx 10^3$–10^2 G. Thus we indeed find (even for the largest values of K_N) that $H_0 = 3.3 \times 10^3$ G is of the order expected for the critical fields, H_c, according to the (perhaps oversimplified) model based upon eq A1–A2. Actually eq A24b leads to a band of k-dependent modes which are excited with different amplitudes as H_0 is increased above H_c. We now must inquire whether the hypothesis of $a \lesssim 1$ is indeed consistent with the result eq A25 and the typical values of the force constants. If one lets $H_0^2 > H_c^2$, e.g., $H_0^2 = 2H_c^2$, this will enhance the values of k^2 such that

$$a_{max} \equiv \frac{LK_N k_{max}^2}{\bar{B}} \approx \frac{K_N^2}{K_1\bar{B}} = (\pi/2\delta_N)^2 \approx 10^{-5}\text{–}10^{-9} \tag{A25}$$

or indeed the weak anchoring limit with respect to the k modes allowed by eq A24c. It then also follows that

$$u_0 \approx A\cos\left[(2a)^{1/2}\left(\frac{z}{L} - \frac{1}{2}\right)\right] \approx A\left[1 - a\left(\frac{z}{L} - \frac{1}{2}\right)^2\right] \tag{A26}$$

In closing this analysis we do wish to note that we have kept α very small to fulfill the inequality of eq A13. However, eq A24c appears to imply an instability, because as α (or A^2) increases, then H_c^2 decreases. Undoubtedly a more complete treatment of the smectic alignment than that of the first term of eq A1 would tend to moderate this instability, but we have already noted that the present theory is only appropriate for the incipient distortions. It would also be appropriate to study the effects of "wetting" or surface tension terms in eq A2.

References and Notes

(1) G. R. Luckhurst and M. Setaka, *Mol. Cryst. Liq. Cryst.*, **19**, 179 (1972); G. R. Luckhurst, M. Setaka, and C. Zannoni, *Mol. Phys.*, **28**, 49 (1974).
(2) (a) F. Pusnik, M. Schara, and M. Sentjurc, *J. Phys. (Paris)*, **36**, 665 (1975); (b) F. Pusnik and M. Schara, *Chem. Phys. Lett.*, **37**, 106 (1976).
(3) (a) Z. Luz and S. Meiboom, *J. Chem. Phys.*, **59**, 275 (1973); (b) Z. Luz, R. C. Hewitt, and S. Meiboom, *ibid.*, **61**, 1758 (1974); (c) S. Hsi, J. Zimmerman, and Z. Luz, *ibid.*, **69**, 4126 (1978).
(4) (a) G. R. Luckhurst and A. Sanson, *Mol. Phys.*, **24**, 1297 (1972); (b) G. R. Luckhurst, M. Ptak, and A. Sanson, *J. Chem. Soc., Faraday Trans. 2*, **69**, 1752 (1973).
(5) (a) D. Sy and M. Ptak, *J. Phys.*, **35**, 517 (1974); (b) *Mol. Cryst. Liq. Cryst.*, **39**, 53 (1977).
(6) (a) W. J. Lin and J. H. Freed, *J. Phys. Chem.*, **83**, 379 (1979); (b) unpublished results.
(7) (a) L. J. Berliner, Ed., "Spin Labeling-Theory and Applications", Academic Press, New York, 1976; (b) S. Schreier, C. F. Polnaszek, and I. C. P. Smith, *Biochim. Biophys. Acta*, **515**, 375 (1978).
(8) K. V. S. Rao, C. F. Polnaszek, and J. H. Freed, *J. Phys. Chem.*, **81**, 449 (1977).
(9) R. J. Birgeneau and J. D. Litster, *J. Phys. Lett.*, **39**, L-399 (1978).
(10) C. F. Polnaszek, C. V. Bruno, and J. H. Freed, *J. Chem. Phys.*, **58**, 3185 (1973).
(11) C. F. Polnaszek and J. H. Freed, *J. Phys. Chem.*, **79**, 2283 (1975).
(12) E. Meirovitch and J. H. Freed, to be published.
(13) E. Meirovitch and Z. Luz, *Mol. Phys.*, **30**, 1589 (1975).
(14) (a) E. Meirovitch, Z. Luz, and S. Alexander, *Mol. Phys.*, **37**, 1489 (1979); (b) *Phys. Rev. A*, **15**, 408 (1977).
(15) (a) P. G. de Gennes, "The Physics of Liquid Crystals", Oxford University Press, New York, 1974; (b) A. Rapini, *J. Phys. (Paris)*, **33**, 237 (1972).
(16) A. J. Dianoux and F. Volino, *J. Phys.*, **40**, 181 (1979).
(17) J. A Murphy, *Mol. Cryst. Liq. Cryst.*, **22**, 133 (1973).
(18) E. G. Rozantsev, "Free Nitroxyl Radicals", Plenum Press, New York, 1970.
(19) J. S. Hwang, R. P. Mason, L. P. Hwang, and J. H. Freed, *J. Phys. Chem.*, **79**, 489 (1975).
(20) J. E. Proust, L. Terminassian-Saraga, and E. Guyon, *Solid State Commun.*, **11**, 1227 (1972).
(21) C. F. Polnaszek, Ph.D. Thesis, Cornell University, 1976.
(22) R. L. Humphries and G. R. Luckhurst, *Chem. Phys. Lett.*, **17**, 514 (1972).
(23) A. J. Leadbetter and E. K. Norris [*Mol. Phys.*, **38**, 669 (1979)] have recently shown in an X-ray study of nematic and smectic phases that the ordering potential is typically well fitted by the form $U = \gamma_2 \cos^2\beta$ and the term $\gamma_4 \cos^4\beta$ is not important.
(24) (a) G. F. Hatch and R. W. Kreilick, *J. Chem. Phys.*, **57**, 3696 (1972); (b) R. W. Kreilick, *ibid.*, **46**, 4260 (1967).
(25) G. R. Luckhurst and C. Zannoni, *Proc. R. Soc. London, Ser. A*, **353**, 87 (1977).
(26) As noted above and as further discussed below, our samples, with $L = 200$ μm, are expected to be practically free from effects of inhomogeneous line broadening due to mosaicity and therefore appropriate for dynamic line shape studies of slow motional spectra, where the magnetic field is tilted relative to the director. We are currently extending the general computer programs to include the much more complex case of nonzero tilt of the field (G. Moro and J. H. Freed, to be published). Such an approach is expected to differentiate between the effects of ordering and those due to changes in the dynamic rates and is especially relevant to the great number of previous observations of CSL in thermotropic and lyotropic smectic crystals,[8] which have been, in most cases, analyzed inadequately, using fast motional theories.
(27) J. S. Hwang, K. V. S. Rao, and J. H. Freed, *J. Phys. Chem.*, **80**, 1490 (1976).
(28) It has recently been shown [A. E. Stillman and J. H. Freed, *J. Chem. Phys.*, **72**, 550 (1980)] that the fluctuating torque model is associated with "collision-induced" torques, while the SRLS model is due to "structure-induced" torques. This supports our belief that the latter is a more suitable explanation for the liquid crystalline anomalies.
(29) (a) P. G. de Gennes, "The Physics of Liquid Crystals", Oxford, New York, 1974, p 289; (b) J. P. Hurault, *J. Chem. Phys.*, **59**, 2068 (1973).
(30) N. A. Clark and R. B. Meyer, *Appl. Phys. Lett.*, **22**, 493 (1973).
(31) J. M. Delrieu, *J. Chem. Phys.*, **60**, 1081 (1974), and references therein.
(32) (a) A. Rapini and M. Papoular, *J. Phys. C4*, **30**, 54 (1969); (b) T. Motooka, A. Fukuhara, and K. Suzuki, *Appl. Phys. Lett.*, **34**, 305 (1979).
(33) R. Courant and D. Hilbert, "Methods of Mathematical Physics", Vol. I, Interscience, New York, 1953, p 210.
(34) L. A. Pipes, "Applied Mathematics for Engineers and Physicists", McGraw-Hill, New York, 1958, p 690.
(35) D. Riviere, Y. Levy, and E. Guyon, *J. Phys.*, **40**, L215 (1979), and references therein.